



A 3D TLM code for the study of the ELF electromagnetic wave propagation in the Earth's atmosphere

Alfonso Salinas^{a,*}, Jorge Porti^b, Enrique A. Navarro^c, Sergio Toledo-Redondo^d,
Inmaculada Albert^d, Aida Castilla^d, Víctor Montagud-Camps^d

^a Department of Electromagnetism and Matter Physics, Research Centre for Information and Communication Technologies (CITIC-UGR), University of Granada, Granada, Spain

^b Department of Applied Physics, Research Centre for Information and Communication Technologies (CITIC-UGR), University of Granada, Granada, Spain

^c IRTIC Institute/ETSE, Universitat de València, Burjassot, Spain

^d Department of Electromagnetism and Electronics, University of Murcia, Murcia, Spain

ARTICLE INFO

Keywords:

Atmosphere electrodynamics
TLM method
Schumann resonances
Full 3D numerical model
Parallel algorithm

ABSTRACT

The interest in the study of electromagnetic propagation through planetary atmospheres is briefly discussed. Special attention is devoted to extremely-low-frequency fields in the Earth's atmosphere for its global nature and possible applications to climate monitoring studies among others. In the Earth's case, the system can be considered as a spherical electromagnetic shell resonator in which two concentric and large conducting spheres with a radius around 6300 km are separated by a very small distance of around 100 km, the atmosphere height. A numerical solution using the Transmission Line Method is proposed. The classical spherical-coordinate description is easy to use, however, the important difference in the dimensions along the three coordinate directions causes high numerical dispersion in the results. A Cartesian scheme with equal node size for all directions is used to reduce this undesired dispersion. A pre-processing stage is the key point introduced to lessen the resulting high demand of memory and time calculation and make the solution feasible. A parallelized Fortran code together with pre- and post-processing Python programs to ease the user interface are provided with this work. Details on the Fortran code and the Python modules are included both in the paper and the source codes to allow the use and modifications by other researchers interested in electromagnetic propagation through planetary atmospheres. The program allows calculation of the time evolution of the electromagnetic field at any point in the atmosphere. It includes the possibility of considering multiple time-dependent sources and different homogeneous and inhomogeneous conductivity profiles to model different situations. Profiles to study day-night asymmetries or locally perturbed profiles which have been attributed to earthquakes in the literature are implemented, for instance.

1. Introduction

Lightning strokes and Transient Luminous Events (TLEs) generated in the upper atmosphere are the main natural sources of the electromagnetic field propagating through the atmosphere and can be considered as the battery of the Global Electric Circuit, the more outstanding part of the Atmospheric Electrodynamics (Rycroft et al., 2008). Lightning strokes and TLEs produce electromagnetic pulses with a short duration, between microseconds and milliseconds, with frequency content in the Extremely Low Frequency (ELF) and the Low Frequency (LF) bands, i.e., with frequencies ranging from a few hertz to

several megahertz (Cooray, 2003).

In the ELF band, the Earth's atmosphere at low altitudes can be considered as a good dielectric, with a conductivity of 10^{-14} S/m, but this conductivity increases with altitude due to the ionizing effect of the cosmic rays. At the D region, at altitudes of about 75–90 km, the conductivity may reach values between 10^{-4} and 10^{-2} S/m, which are comparable with the conductivity at the Earth's crust. The electromagnetic model for the Earth at the ELF band approximates the atmosphere as a spherical shell resonator. The inner and outer limits are considered as perfectly conducting surfaces, while the medium between both plates is filled with an inhomogeneous conducting material. This

* Corresponding author.

E-mail address: asalinas@ugr.es (A. Salinas).

<https://doi.org/10.1016/j.cageo.2023.105499>

Received 21 September 2023; Received in revised form 28 November 2023; Accepted 29 November 2023

Available online 5 December 2023

0098-3004/© 2023 The Authors. Published by Elsevier Ltd. This is an open access article under the CC BY-NC-ND license (<http://creativecommons.org/licenses/by-nc-nd/4.0/>).

model in the Earth's case is a challenging one due to the important difference between its perimeter, around 40,000 km, and the ionosphere height, around 60–100 km. This makes the system an electromagnetic resonant cavity in which the ELF components of the lightning strokes and TLEs may travel several turns around the Earth to form a stationary wave, resonating at certain specific frequencies in this range. These frequencies are known as Schumann Resonances (SRs) after Schumann who first predicted them in 1952 (Schumann, 1952). SRs at the Earth occur at approximated values of 8, 14, and 21 Hz for the first three resonant modes and can be observed at any point on Earth, although the associated electromagnetic field is very weak and is easily masked by the anthropogenic noise (Fornieles-Callejón et al., 2015; Nickolaenko and Hayakawa, 2002). This low amplitude explains why SRs were not experimentally detected until 1960 (Balsler and Wagner, 1962). A thorough historical revision on SRs can be found in (Besser, 2007), while theoretical and experimental aspects are presented in (Nickolaenko and Hayakawa, 2002, 2014). Interesting subsequent reviews can also be found in (Price, 2016; Sători et al., 2013; Simões et al., 2012).

The interest in SRs relies in the fact that they have applications in the monitoring of climate changes. In this sense, the relation between SR variations and the average temperature of the surface near tropical latitudes is described in (Williams, 1992) and strengthened by (Füllkrug and Fraser-Smith, 1997). The climate change of the Earth has the lightning activity as a climate variable. Recent contributions to the reconstruction of global lightning activity based on SRs can be found in (Prácser et al., 2019; Williams et al., 2014). Another important topic is the solar effects on SRs, which are discussed in (Bozóki et al., 2021; Nickolaenko et al., 2015; Rodríguez-Camacho et al., 2022; Salinas et al., 2016; Sători et al., 2016). A recent publication by Williams et al., (2021) proposes the monitoring of variations in the SR intensity to predict extreme climate events such as the Super El Niño. Others examples concerning climate phenomena are applied to the study of year scale fluctuations at the ionosphere (Koloskov et al., 2020) and references therein. These and other works suggest the use of SRs to monitor climate changes. The study and the characterization of modifications in SRs due to natural phenomena or anthropogenic activities provide information not only on the external agent producing a variation in the observed SRs, but also inform about the magnitude of these agents. This interest is not only of fundamental scientific nature to understand the Physics behind atmospheric electrodynamics, but it is also of practical interest in the design of experimental equipment or in optimizing a measuring campaign, for instance. In this sense, the numerical calculation of SRs at Titan carried out by (Morente et al., 2003b) was a collaboration with members of the Space Research Institute of Austrian Academy of Sciences to obtain information which could help in the design of the probe to measure these resonances at Titan during the NASA-ESA Cassini-Huygens mission, first launched at 1997. The study of resonances at Mars under different dust scenarios presented in (Toledo-Redondo et al., 2017) was intended to provide valuable input information to help in the measurement of SRs at Mars during the ESA ExoMars mission, which was first launched at 2016. As a final example of the applicability of SR studies, let us mention that an important part of any engineering project is the use of appropriated tools to objectively determine the effectivity of the proposed activities (Koley, 2023). In this sense, analytical or numerical tools to study RSs at the Earth may be incorporated in broader engineering projects devoted to environmental or sustainability improvements, for instance, as numerical or analytical assessment tools to determine the effectivity of the activities proposed in the project.

The study of the SRs in the Earth can be carried out by means of semi-analytical methods, such as the zonal harmonic series representation, (Nickolaenko and Hayakawa, 2002), which can be considered in both the time and the frequency domain. Regarding the attempts to numerically model this problem, the main numerical difficulty arises from the important difference between one dimension and the other two. In such a situation, the three-dimensional (3D) problem can be modeled through a two-dimensional (2D) scheme. This causes that Maxwell's equations

are approximated by Kirchhoff equations in the form of the 2D Telegrapher's Equations (2DTE) relating voltages and intensities propagating through a 2D transmission line mesh with spherical geometry (Madden and Thompson, 1965), i.e., disregarding changes with altitude. These approximated equations are analytically solved in the papers by (Bozóki et al., 2019; Galuk et al., 2019, 2020; Kirillov, 1996; Prácser et al., 2019), while a numerical solution using the Finite Elements method is presented in (Kulak et al., 2003).

The 2DTE approaches mentioned above allow solving simplified situations in which variations with height are negligible or averaged, but other numerical schemes are required if the variations of conductivity with height are to be modeled. Finite Differences in the Time Domain (FDTD) or the Transmission Line Matrix (TLM) methods have been used to solve these situations. In order to reduce the high numerical requirements, the initial works using FDTD considered excitation of the Earth cavity at the poles to allow using azimuthal symmetry. This is the case of the works by (Cummer, 2000; Holland, 1983; Hayakawa and Otsuyama, 2002; Otsuyama et al., 2003; Simpson and Taflove, 2002; Soriano et al., 2005). Analogous works for other planets and moons are presented in (Navarro et al., 2007; Soriano et al., 2007; Yang et al., 2006).

The works by (Simpson and Taflove, 2004; Yang and Pasko, 2005; Yang et al., 2006) report the first full-3D-FDTD models of the cavity in which no symmetry considerations are imposed. A detailed review of the FDTD application to SR calculations can be found in (Simpson and Taflove, 2007). Subsequent works on other topics related with SRs are presented in (Marchenko et al., 2022; Navarro et al., 2008; Yu et al., 2012).

TLM method is another numerical method successfully applied to solve electromagnetic problems. TLM is not a purely mathematical numerical method, since it is not intended to solve analytical equations governing the phenomenon under study. The TLM method substitutes the original medium by an analogous transmission line mesh, instead. The electromagnetic field in the actual system is studied by means of voltage and current pulses propagation in this analogous mesh (Christopoulos, 1995). The transmission line knowledge required in TLM has caused that most of its applications are concentrated on electromagnetic problems of different types, such as waveguides or electromagnetic compatibility problems (Christopoulos, 1995), but other applications have been reported in Acoustics and Diffusion (Portf and Morente, 2001; de Cogan, 1998). The versatility of the TLM method to deal with materials with general properties was presented in an elegant and general formulation by (Paul et al., 1999a, 1999b, 2002). This interest in the improvement of the TLM method and its application to more challenging situations is still in the basis of more recent publications (Ijeh et al., 2021; Portf et al., 2021; Tronchoni et al., 2019).

Despite the difficulty introduced by the use of analogies when compared to a purely mathematical method such as FDTD, the TLM conceptual approach presents some specific advantages in challenging situations. An example is the modelling of thin wire antennas. While FDTD requires the use of a node with a size comparable to the antenna radius, TLM allows using a coarse mesh by defining an equivalent circuit for the antenna which is added to the TLM node describing the medium in which the antenna is located (Portf et al., 1992). A second example is the numerical modelling of a metamaterial with negative values of both the electric permittivity and the magnetic permeability. The TLM solution resembles the way in which metamaterials are experimentally implemented, changing capacitive by inductive elements and vice versa (Smith et al., 2000). Therefore, TLM introduces most of the physical consequences of this change for all frequencies (Blanchard et al., 2008), while the direct FDTD solution may introduce causality problems since the dispersion properties are not easily included (Ziolkowski and Kippel, 2003). Some details on the TLM method will be presented in Section II.

As with the FDTD method, TLM was initially applied to solve 3D problems under azimuthal symmetric excitation conditions, which reduced the problem to a 2D one but including height-dependent

conductivities (Morente et al., 2003a). Subsequent works considered the study of SRs for other celestial objects (Molina-Cuberos et al., 2006; Morente et al., 2003b).

The FDTD and TLM models mentioned above were formulated in a spherical coordinate system. It seems the natural way, since it perfectly fits the geometry of the problem and it is suitable for spherical cavities in which all dimensions are comparable. But our situation is that azimuthal and zenithal lengths are two orders of magnitude greater than the radial length. The FDTD or TLM unit cell is extremely thin in the radial direction compared with the other two dimensions, causing an important numerical dispersion to appear. The solution seems evident: Cartesian coordinates should be used, with equal length for the three directions, thus producing a reduction of numerical dispersion. The staircase approximation is not relevant due to the high values of the wavelengths under interest, the ELF region. However, a direct Cartesian algorithm modeling a cubic region would be extremely inefficient, since most cells would lie outside the region of interest, located between two large spherical plates separated by a very small distance. The first study presenting a full 3D formulation in Cartesian coordinates was presented in (Toledo-Redondo et al., 2013). The work included a pre-processing stage in which all the nodes in a 3D region were classified to identify the points located inside the cavity and the nodes with which they were connected. This stage avoided dedicating storage and time-computing resources to nodes outside the atmosphere. This initial study was later applied to carry out specific studies of SRs at the Earth (Toledo-Redondo et al., 2016) and Mars (Toledo-Redondo et al., 2017).

In this work, the authors present and make available to the scientific community a full 3D Cartesian code for the modelling of ELF propagation through planetary atmospheres with a radial dimension which is much lower than the other two dimensions. The program provided allows calculating the electromagnetic field at any point in the atmosphere under different situations. The program has applications in the study of the atmosphere electrodynamics in general and, more specifically, in the numerical study of the RS regular behavior and their variations when external perturbations occur, such as those due to solar activity, day-night asymmetry or earthquake activity, for instance. It allows characterization of the effect of different agents and the extent of this effect on the SRs, to help determining the magnitude of the agent altering the SRs, which may help in designing equipment, planning measurement campaigns or assess the effectiveness of particular activities included in environmental projects, for instance. In this sense, the aim of presenting and sharing this code is mainly twofold. In one hand, it may help to experimental researchers in SRs, for instance, to obtain independent numerical results to be compared to their experimental findings. On the other hand, as the source Fortran and Python codes are provided with this paper, numerical researchers in atmospheric electrodynamics may adapt them to their own numerical calculations or experimental facilities and introduce additional particular improvements. The code is based on the work previously reported by the authors in (Toledo-Redondo et al., 2016), together with improvements presented subsequently in (Salinas et al., 2015) and in (Portí et al., 2021). The code is written in Parallelized Fortran using OpenMP directives, with some parts developed in Python to ease the interface between the computer and the user.

The paper is organized as follows. The electromagnetic problem and the fundamentals of the TLM numerical methodology are described in Section 2. The main parts of the Fortran code are presented in Section 3. Some conductivity models of the Earth's atmosphere are presented in Section 4, while results concerning these models are shown in Section 5. Finally, Section 6 summarizes the main conclusions of this work.

2. The electromagnetic problem and its solution using the TLM method

The system considered is a spherical shell defined by the Earth's surface and the lower ionosphere, both limits considered as perfect

conductors, and filled with the atmosphere, an isotropic and inhomogeneous dielectric with low conductivity values. The system is driven by current sources which model lightning strokes. The sources present a Gaussian-shape time evolution, with important content at low frequencies, below 100 Hz in the Earth's case. As mentioned previously, despite the spherical geometry of the system, Cartesian coordinates will be used to reduce numerical dispersion.

The task is solving Maxwell's equations in the time domain with the perfectly conducting boundary conditions at the shell limits, in order to obtain the time evolution of the electromagnetic field at any point in the atmosphere. The SRs, for instance, can be obtained from these EM fields using Fourier transform. The program code is designed to allow obtaining the SRs in particular cases of interest, which include different atmospheric conductivity profiles, local perturbations of the conductivity, day-night asymmetry or multiple sources, among others.

Concerning the numerical method used, TLM is a low frequency method which models an electromagnetic problem from a conceptual point of view more than from a purely mathematical one. The method discretizes time and space. The full medium is substituted by an analogous transmission line mesh formed by the connection of elementary transmission line circuits, the TLM nodes, each node substituting a small volume of the original medium. Voltage and current pulses propagate in this mesh in a manner analogous to that of the field in the original medium. In its basic 3D scheme, the nodes consist of 12 transmission lines which model the propagation for all polarizations along the three Cartesian directions, in both the positive and the negative directions. These lines are termed the link lines and connect to link lines of adjacent nodes to model propagation. Extra lines can be added to adjust permittivity, permeability, or conductivity, through capacitive, inductive or resistive stubs, respectively. The topology of the node depends on the particular problem to solve, but the TLM algorithm is conceptually simple: at each time calculation, a set of voltage or current pulses reach the node centers, they are scattered according to Maxwell's equations and produces a set of reflected pulses. These reflected pulses spend one timestep, Δt , in propagating through the node lines to reach the center of adjacent nodes in the case of link lines or the same node in the case of capacitive or inductive stubs. The pulses reflecting to resistive lines are lost, thus modelling the electric losses by Joule effect.

The program presented with this work uses the basic 3D formulation shown in Fig. 1 and described in (Salinas et al., 2015), with only 12 link lines, including lossy effects but neither inductive nor capacitive stubs. The node has a cubic shape with a size of Δl . A remarkable property is that the node is symmetrical and all the field components are defined at the node center at the same instant, and this is the reason why the node is known as the Symmetrical Condensed Node (SCN) (Christopoulos, 1995; Johns, 1987). The link lines are defined through a set of 3 indexes, (j, s, k) , where $j = \{x, y, z\}$ describes the direction of propagation, $k = \{x, y, z\}$ indicates the polarization, and $s = \{p, n\}$ indicates if the line is in the positive or negative side, respectively. The characteristic impedance of the link lines, Z_0 , relates the incident voltage and current pulses at any line (j, s, k) through $I_{jsk}^i = V_{jsk}^i / Z_0$. In this node, Z_0 equals the vacuum impedance and the timestep is related to the node size according to $\Delta t = \Delta l / (2c)$, c being the vacuum speed of light. The orange cubic box at the center indicates that connections are to be understood in a formal sense to describe the coupling between Maxwell's equations.

Vector Maxwell's equations are a set of six coupled scalar differential equations. Similarly, the 3D SCN of Fig. 1 may be split into six 2D sub-circuits: three series and three parallel circuits. Each series circuit defines a common current and is related to a component of the magnetic field through that specific component of Ampère's law. Each parallel circuit defines a common voltage and is related to a component of the electric field through the corresponding component of Faraday's law. Fig. 2 shows the series circuit for H_x and the parallel circuit for E_x (Salinas et al., 2015). Each component of Ampère's law is coupled to two components of Faraday's law. Similarly, each series circuit is coupled to

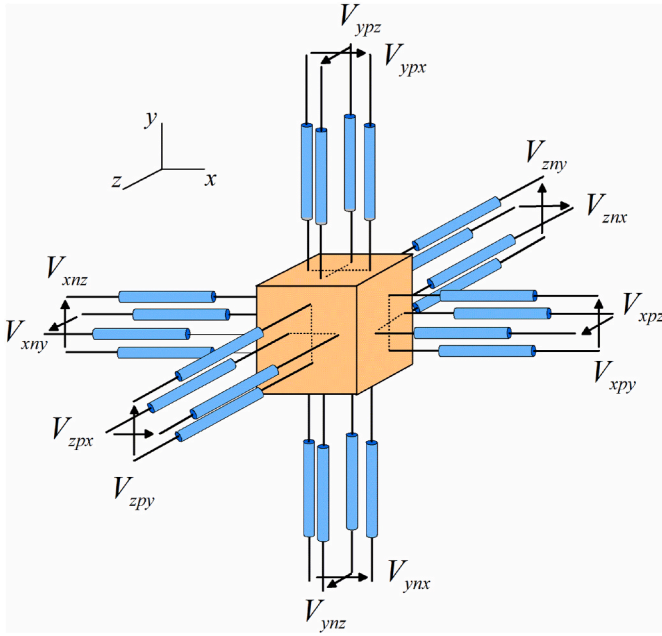


Fig. 1. Geometry of the 3D TLM Symmetrical Condensed Node. Each line defines a component of the electric and the magnetic field propagating along a particular direction. The orange box at the center indicates that connections are to be understood as formal ones to describe the coupling existing between the different components of the vector Maxwell's equations.

a pair of parallel circuits. Conversely, each parallel circuit is coupled to a pair of series nodes. These formal couplings are shown in Fig. 2 with orange boxes.

As regards the series circuit, its total impedance is $Z_T = 4Z_0$. The incident voltage pulses define the circuit current, I_x , and the corresponding magnetic field, as

$$I_x = \frac{H_x}{\Delta l} = \frac{2}{Z_T} (V_{zpy}^i - V_{zny}^i - V_{ypz}^i + V_{ynz}^i). \quad (1)$$

Concerning the parallel circuit, it has a total admittance of $Y_T = 4Y_0 + G_x$, where $Y_0 = 1/Z_0$ and G_x models the electric losses related to E_x through the infinitely-long line with voltage V_{σ_x} . In this case, the current pulses are the natural quantities and the global circuit voltage and its associated electric field are

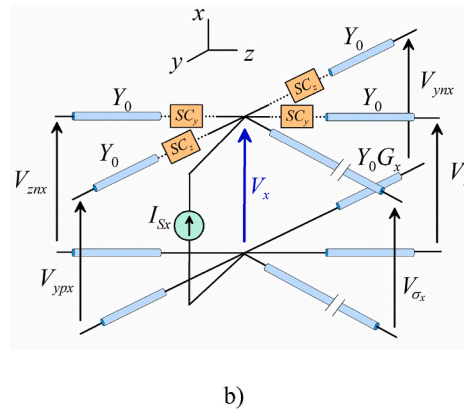
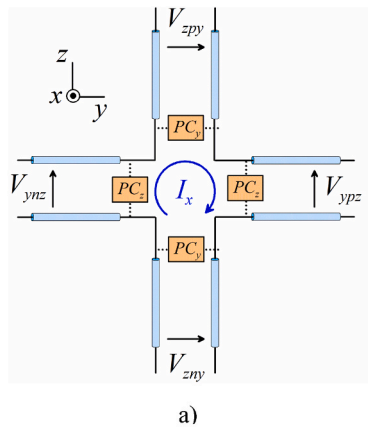


Fig. 2. a) Series circuit for H_x . Orange boxes describe a formal coupling with the parallel circuits which define E_y and E_z . b) Parallel circuit to define E_x . The circuit is formally coupled (orange boxes) to the series circuits for H_y and H_z . Global circuit quantities, I_x and V_x , define the corresponding field quantities, H_x and E_x , respectively.

$$V_x = \frac{E_x}{\Delta l} = \frac{2}{Y_T} (I_{ypx}^i + I_{ynx}^i + I_{zpx}^i + I_{znx}^i) + \frac{I_{Sx}}{Y_T} = \frac{2}{Y_T Z_0} (V_{ypx}^i + V_{ynx}^i + V_{zpx}^i + V_{znx}^i) + \frac{I_{Sx}}{Y_T}, \quad (2)$$

where I_{Sx} stands for the source electric current along the x-direction. Once the circuit quantities in (1) and (2) are obtained for the three Cartesian directions, the reflected voltage pulses may be easily calculated. For the y-polarized lines along the z-direction, it results (Salinas et al., 2015)

$$V_{zpy}^r = V_y - Z_0 I_x - V_{zny}^i, V_{zny}^r = V_y + Z_0 I_x + V_{zpy}^i. \quad (3)$$

Analogous expressions can be derived for the rest of link lines.

3. The algorithm details

As mentioned before, the system consists of two very large and concentric perfectly-conducting spheres with radius R_1 and $R_2 = R_1 + h$, respectively, $h \ll R_1$ being the ionosphere height. Both spheres are included inside a cubic TLM mesh with a side of $2R_2$. This Cartesian scheme is easy to program through a 3D array, allows a direct knowledge of the adjacent nodes and reduces numerical dispersion. However, the very low value of h compared with that of R_1 causes that most of the TLM nodes in this cubic region lie outside the atmosphere and, therefore, they should be neither stored nor modeled. The inclusion of a pre-processing stage to eliminate these unnecessary nodes and transform the original 3D array of the cubic Cartesian scheme to a 1D array of reindexed nodes is the key point which makes it possible to numerically model such a challenging problem in an efficient way.

The algorithm is developed in three main blocks:

1. Transformation of the coordinates.

The input data are provided at this stage, among them, the location of sources and output field points. These points are referred to the Earth's surface. The program 'Input_Earth_box.py' translates them to Cartesian coordinates referred to the cubic TLM mesh.

2. Pre-processing stage: reindexing and node characterization stage.

The code 'Earth_TLM_main.f95' identifies the points inside the atmosphere and their electromagnetic properties, assigns new appropriated indexes to them and identifies the indexes of the adjacent nodes as well as nodes at the conducting limits of the problem. This identification will ease the conversion of reflected to incident pulses at the next

timestep. As a result of this stage, the 3D scheme has been converted to a 1D scheme.

3. The marching-on in time TLM process ‘*Earth_TLM_MoiT.f95*’.

For each timestep and indexed node, the set of reflected voltage pulses are obtained from the corresponding set of incident pulses using equations (1)–(3). The output fields at the desired points are calculated and stored at this stage. The corresponding Fortran 95 code has been parallelized using a shared memory architecture with OpenMP directives.

Let us describe the fundamental details of each block in the following subsections.

3.1. Transformation of the coordinates (code ‘*Input_Earth_box.py*’)

At the first block, the input parameters for the problem are provided through the file *input_Earth.txt*. Namely, the following data are included:

1. Number of total timestep calculations
2. Side length of the cubic TLM node.
3. Earth’s radius (inner cavity radius)
4. Inner ionosphere radius (outer cavity radius).
5. A code number to select the atmosphere conductivity profile (described later).
6. Number of source points.
7. Source coordinates referred to the Earth’s surface: altitude, zenithal and azimuthal angles in degrees.
8. Orientation of the current density at each source point, expressed in spherical components.
9. Number of output points.
10. Coordinates of the output points referred to the Earth’s surface: altitude, zenithal and azimuthal angles in degrees.

The Python code ‘*Input_Earth_box.py*’ reads the data from the file ‘*input_Earth.txt*’, it converts them to Cartesian coordinates referred to the Cubic Cartesian TLM mesh and, finally, stores them in a new file named ‘*input_box.txt*’ used in stage 2.

3.2. Pre-processing stage (code ‘*Earth_TLM_main.f95*’)

The aim of this second block is twofold:

1. A 1D array is defined containing the indexes corresponding to the nodes at the boundary of the system, i.e., the nodes adjacent to the Earth’s surface and the ionosphere.
2. The identification of the pair of indexes corresponding to adjacent lines, whose reflected voltage pulses will be exchanged to produce the incident pulses at the next timestep.

This part is developed according to the following scheme:

Step 1: Characterization of the nodes: indexation, boundary and neighbor nodes.

The first task is the indexing of the nodes in the total cubic region which are located inside the much smaller atmospheric region. For the Earth’s case, with an inner radius of 6370 km and an ionosphere height of 100 km, a node size of $\Delta l = 10$ km requires using a total of $1274^3 \approx 2.17 \cdot 10^9$ nodes in the global cubic region. However, due to the fact that the height is two orders of magnitude lower than the Earth’s radius, only around $5.18 \cdot 10^7$ nodes are located in the region of interest, the atmosphere. This reduction to approximately 2.4 % of the original nodes causes an important reduction in both the time calculation and the memory storage requirements which turns the unaffordable original numerical model into a feasible one.

Since the code considers inhomogeneous conductivities, a new array with the conductivity value at each newly indexed node is defined at this moment. The different conductivity profiles implemented are discussed in section 4. The last process in this step is identifying the new indexes corresponding to source and output points.

It is worth noting that this is the part which requires a more demanding use of time calculation and memory resources. But this expensive task is only carried out once. As a result, it generates output arrays of reduced memory, with reindexed location and properties of nodes. Most of the auxiliary memory used in this process is not needed in subsequent stages and is released by means of proper DEALLOCATE Fortran sentences at the end of this procedure.

Step 2. Identification of adjacent lines.

At this point, we are aware of the nodes we are interested in, but each node contains 12 lines connecting adjacent nodes. The next step identifies which lines in one node are connected to lines in other nodes to ease the conversion of reflected pulses to incident pulses for the next time iteration. To do so, two new arrays are defined. The first one contains the indexes of those lines connected to the inner and outer conducting boundaries. The second array stores the pairs of lines connected, a total of $6.21 \cdot 10^8$ lines if $\Delta l = 10$ km. It is worth noting that a minimum node size of 6.6 km is required in the provided Fortran code for the Earth’s atmosphere, which is limited by the fact that the number of lines must be lower than 2^{31} , which is the maximum value for the standard 4-byte integer variables used in the code. For better resolutions, the integer variables in the code should be adapted to 8-byte integer type.

Step 3: Source implementation and numerical limit on frequency

The time-dependence of the source function is defined at this point. Since TLM is a time domain numerical method, it is appropriated to use a time-dependent function containing a wide frequency spectrum. For its similarity with electromagnetic pulses generated by lightning strokes and TLEs, the Gaussian excitation is often used. It may be expressed as

$$g(t) = e^{-g^2(t-t_m)^2}, \quad (4)$$

where t_m is used to avoid excitation at $t < 0$ and g is chosen to control the time width. The Fourier Transform of (4) is given by:

$$G(f) = e^{-i 2\pi f t_m} \frac{\sqrt{\pi}}{g} e^{-\pi^2 f^2 / g^2}, \quad (5)$$

where f stands for frequency. If the spectral content is defined by the frequency, f_{maxg} , at which the amplitude of $G(f)$ is one tenth of the maximum value, it results that $f_{maxg} \approx 0.5g$.

It is important to bear in mind that the maximum frequency excited should be properly modeled by the numerical method. It is a well-known fact that spatial discretization produces numerical dispersion, which limits the frequency for the valid numerical results. A usually accepted criterium for valid frequency results is that the minimum corresponding wavelength is sampled at least ten times (Morente et al., 1995; Ijeh et al., 2021). Therefore, a specific node size, Δl , ensures acceptable results for frequencies below a frequency $f_{max\Delta l}$ given by:

$$f_{max\Delta l} = \frac{c}{10\Delta l}. \quad (6)$$

The values of g and Δl should be chosen so that $f_{maxg} \leq f_{max\Delta l}$.

Step 4: Program outputs

Two output files are generated: ‘*geometry1*’ and ‘*geometry2*’ and used in step 3. The former is a text file which summarizes the input data, whereas the later contains auxiliary arrays resulting from step 2 in

binary format.

3.3. The marching-on in time TLM process 'Earth_TLM_MoiT.f95'

The third block of the presented code calculates the electric and magnetic field at each node and time iteration. It is split into the two distinct parts mentioned before: i) reflection of incident pulses and, ii) transmission of reflected pulses and conversion to incident ones at adjacent nodes at the next timestep.

Regarding the first process, the incident pulses applied to equations (1) and (2) provide the voltage at the parallel nodes and the currents at the series nodes, respectively. Then, the set of reflected voltage pulses at each line will be obtained using (3). The excitation at source points is implemented at this moment.

Output information is provided in two files:

1. *Voltages_box*. A binary file contains the voltage and current at the parallel and series nodes of each 3D TLM output node, respectively. These magnitudes correspond to the electric and magnetic fields in arbitrary units.
2. *Time_box*. A formatted file with the total CPU time spent in the calculation.

This block is parallelized using OpenMP directives, which basically consists of using OMP DO sentences for the node index loops, since the time sequence cannot be parallelized.

4. Conductivity profiles implemented in the code

The conductivity, σ , at each node can be defined through the input conductivity code number at the fifth line of the input file 'input_Earth.txt' described in section 3.1. Five conductivity profiles are modeled. The zero and one values correspond to a homogeneous atmosphere with $\sigma = 0$ and $\sigma = 10^{-10}$ S/m, respectively.

Other three values of the conductivity codes, 10, 11 and 12, are also possible. They implement the following two-exponential conductivity profile (Toledo-Redondo et al., 2016):

$$\sigma(z) = \begin{cases} \sigma_{kn} e^{(z-h_{kn})/\xi_a} & \text{if } z < h_{kn}, \\ \sigma_{kn} e^{(z-h_{kn})/\xi_b} & \text{if } z \geq h_{kn}, \end{cases} \quad (7)$$

where z stands for the height, $\sigma_{kn} = 2\pi f_{kn} \epsilon_0$ and $f_{kn} = 10$ Hz, and ϵ_0 is the vacuum permittivity. The rest of magnitudes in (7) are specified in Table 1 to describe three usual profiles:

- The global two-exponential profile (conductivity code number = 10). The conductivity is only height-dependent.
- The day-night two-exponential profile (conductivity code number = 11). The conductivity profile distinguishes a day and a night region. One half of the atmosphere uses day-side parameters ($0^\circ \leq \varphi < 90^\circ$ and $270^\circ \leq \varphi < 360^\circ$), while the other side has the night-side parameters ($90^\circ \leq \varphi < 270^\circ$).
- Finally, the earthquake perturbed profile (conductivity code number = 12) proposed in (Galuk et al., 2020). The conductivity profile is that of profile 10 except for a limited region, with zenithal angles lower than 27° , with data perturbed by an earthquake occurring at the North Pole.

5. Results

This section illustrates some of the examples which can be modeled with the code supplied with this work. All the cases presented use a node size of 10 km and a total of $N_t = 2^{15}$ time calculations, except where otherwise noted. The timestep is $1.6678 \cdot 10^{-5}$ s and the frequency increment is around $\Delta f = 1/(N_t \Delta t) = 1.8$ Hz. This node size ensures valid results for frequencies below 3 kHz, approximately. A Gaussian

Table 1
Two-exponential profiles.

Parameter	Global two-exponential profile (Conductivity code number = 10)	Day-night two-exponential profile (Conductivity code number = 11)	Earthquake perturbed profile (Conductivity code = 12)
σ_{kn} (S/m)	$5.56 \cdot 10^{-10}$	$5.56 \cdot 10^{-10}$	$5.56 \cdot 10^{-10}$
h_{kn} (km)	55		55
h_{kn} day (km)		54	
h_{kn} night (km)		60	
ξ_a (km)	8.3		8.3
ξ_a day (km)		7.5	
$(0^\circ \leq \varphi < 90^\circ$ and $270^\circ \leq \varphi < 360^\circ)$			
ξ_a night (km)		9.1	
$(90^\circ \leq \varphi < 270^\circ)$			
ξ_a quake (km)			13
ξ_b (km)	2.9		2.9
ξ_b day (km)		2.7	
ξ_b night (km)		3.8	
ξ_b quake (km)			2.0
$(\theta \leq 27^\circ)$			

vertical current source is applied at ground level at an equatorial point ($\theta = 90^\circ, \varphi = 0^\circ$) with $g = 2 \cdot 10^3 \text{ s}^{-1}$, which excites frequencies of up to 1 kHz. With the time calculations chosen, the signal completes four full perimeters around the Earth, which is enough for the lossy atmospheres considered. A longer calculation is required for a better modelling of the ideal case with zero conductivity in which no attenuation is present.

The first example considers a homogeneous atmosphere in two cases: $\sigma = 0$ and $\sigma = 10^{-10}$ S/m. Fig. 3 is a plot of the vertical electric field versus time at ground level, $\theta = 45^\circ, \varphi = 0^\circ$. Results are in good agreement with those reported in (Toledo-Redondo et al., 2016). It becomes clear the attenuation effect caused by the conductivity (red line) which is not present in the ideal case (black line). The frequency domain fields are plotted in Fig. 4 in which the usual values for the SRs are clearly observed. Results for different number of time calculations are considered to illustrate their effect on the frequency resolution. It must be noted that the case with for $\sigma = 10^{-10}$ S/m does not actually require all those calculations to be carried out. It is enough to directly adding

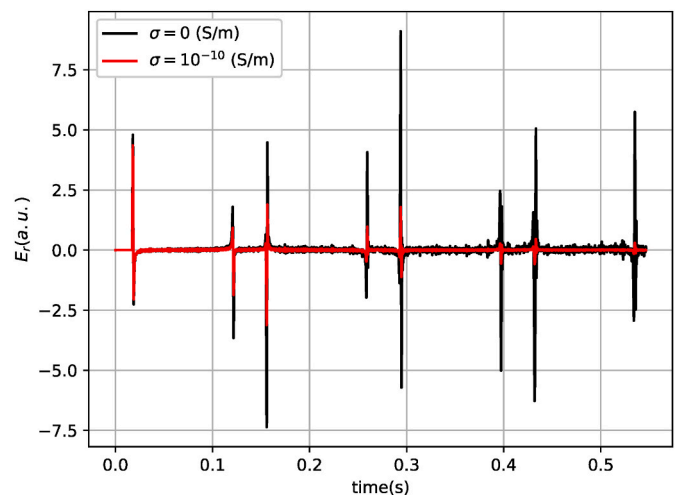


Fig. 3. Vertical electric field versus time at a point located at ground level, $\theta = 45^\circ$ and $\varphi = 0^\circ$ for an ideal atmosphere (black line) and a homogeneous conductivity of $\sigma = 10^{-10}$ S/m (red line) when a Gaussian vertical current is excited at ground level, $\theta = 90^\circ$ and $\varphi = 0^\circ$.

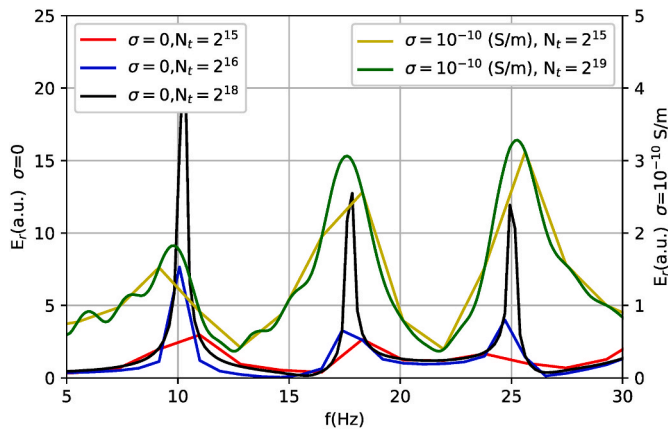


Fig. 4. Vertical electric field versus frequency at ground level, $\theta = 45^\circ$, $\varphi = 0^\circ$ for an ideal atmosphere (left axis) and a homogeneous conductivity of $\sigma = 10^{-10}$ S/m (right axis) when a Gaussian vertical current is excited at ground level, $\theta = 90^\circ$ and $\varphi = 0^\circ$. Different total time calculations are plotted to show their effect on the Fourier Transform.

zeroes once the time-domain signal has been sufficiently attenuated.

The next case considers the global two-exponential profile. Fig. 5 shows the NS component of the magnetic field versus time at ground level for different output points specified by $\theta = 45^\circ$, and several values of φ , from 0° to 180° . The delay and attenuation between the different output signals are clearly observed, together with a certain widening of the signal caused by dispersion. The solid lines in Fig. 6 show the frequency domain results. The dash-dotted lines show the slight variation caused by the earthquake perturbed profile.

Next, the effect of considering day-night asymmetry in the atmosphere conductivity (profile code number = 11) is shown in Fig. 7 for the frequency-domain EW magnetic-field component. The source is located at ground level, at the Equatorial line in the middle of the day side ($\varphi = 0^\circ$). Day side points correspond to $\varphi < 90^\circ$ and night-side points correspond to $\varphi \geq 90^\circ$. The dash-dotted lines show the field for the day-night two-exponential profile, while the global two-exponential profile case is plotted with solid line for comparison.

Finally, Fig. 8 shows the time evolution of the NS magnetic field generated at ground level by two simultaneous sources, one at ground level and other at an altitude of 60 km, typical locations for a lightning stroke and a TLE, respectively. Fig. 9 is the corresponding frequency-domain plot. It is worth noting the deviation from the case shown in

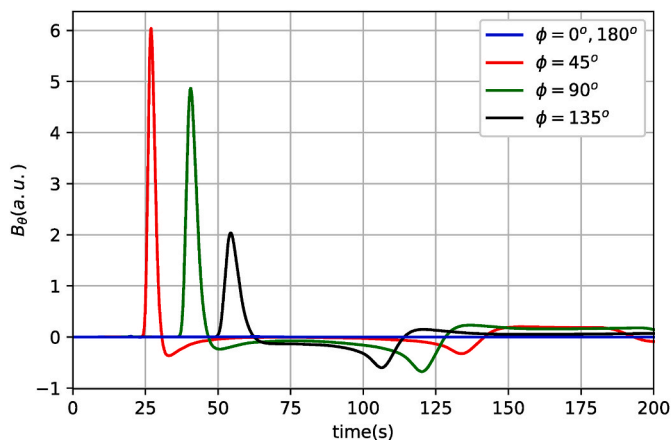


Fig. 5. Time evolution of the NS component of the magnetic field for the global two-exponential conductivity profile of Table 1. A vertical Gaussian current source is excited at ground level, $\theta = 90^\circ$ and $\varphi = 0^\circ$, while output points are defined at ground level, $\theta = 45^\circ$ and several values of φ , from 0° to 180° .

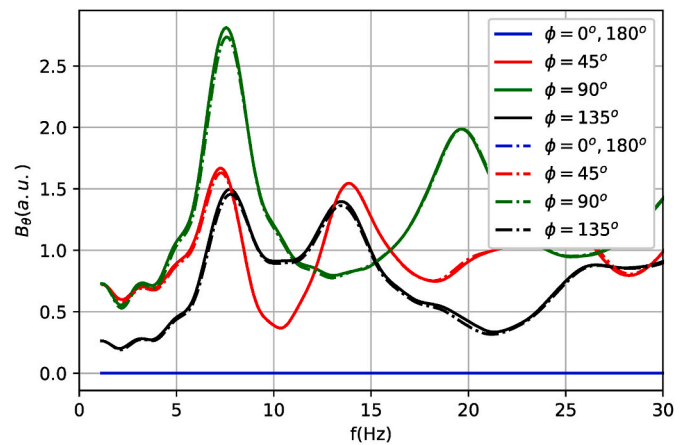


Fig. 6. Frequency-domain NS component of the magnetic field in response to a Gaussian vertical current source excited at ground level, $\theta = 90^\circ$ and $\varphi = 0^\circ$. Output points are defined at ground level, $\theta = 45^\circ$ and several values of φ , from 0° to 180° . Solid lines show the case of the global two-exponential conductivity profile of Table 1 (profile code number = 10), while dash-dotted lines describe the same profile perturbed by an earthquake (profile code number = 12).

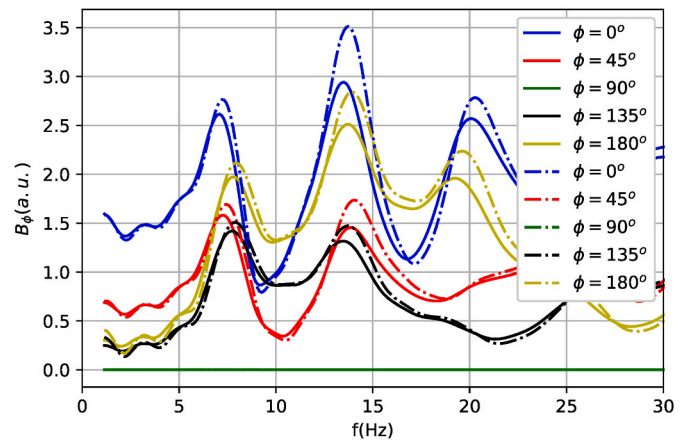


Fig. 7. Frequency-domain EW component of the magnetic field for the two-exponential conductivity profile (solid lines) and the day-night two-exponential conductivity profile (dash-dotted lines). The source is located at the Equatorial line, ground level, in the middle of the day side ($\varphi = 0^\circ$). Outputs at the day side correspond to $0^\circ \leq \varphi < 90^\circ$. The night side points have $90^\circ \leq \varphi \leq 180^\circ$.

Figs. 5 and 6 with one source. For more details on this and previous figures, please see the notebooks provided with this work.

To briefly summarize this section, the examples considered above are intended to illustrate the versatility of the provided code to numerically solve different situations of interest in the Earth’s atmospheric electro-dynamics field. The homogeneous and the global two-exponential fields provide information about the resonant cavity itself. The day-night asymmetric profile may contribute to the study of the solar activity influence on SR variations. Finally, the locally perturbed profiles may model the effect of local events, such as earthquakes or others, on the RSs. As pointed out in (Sátori et al., 2016): “Future analysis of major perturbations of the SR will benefit from the use of a cavity model with both day-night and polar asymmetry, and a common processing of all receiver data sets for the same modal frequencies”. The expected changes in RS when considering different situations, solar activity or differences in conductivity profiles, for instance, can also be studied, which may help in linking the observed changes and the agents causing these changes. In this sense, the use of the numerical code provided with this work may contribute to a better knowledge of the atmospheric electro-dynamics and to monitoring some aspects of climate changes,

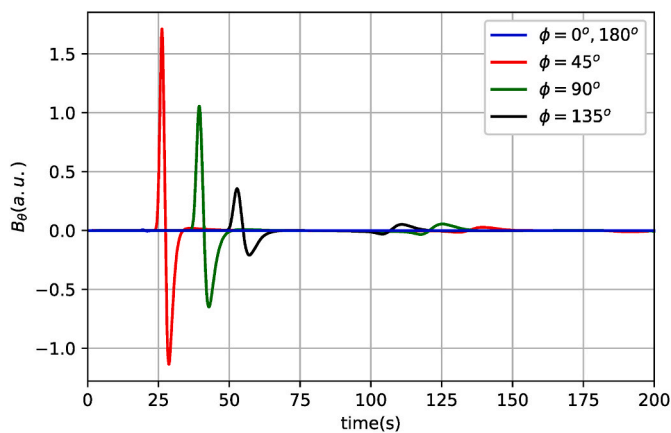


Fig. 8. NS magnetic field versus time for two simultaneous sources, one at ground level and the other at an altitude of 60 km with $\theta = 90^\circ$ and $\varphi = 0^\circ$. Output points are defined at ground level, $\theta = 45^\circ$ and several values of φ , from 0° to 180° .

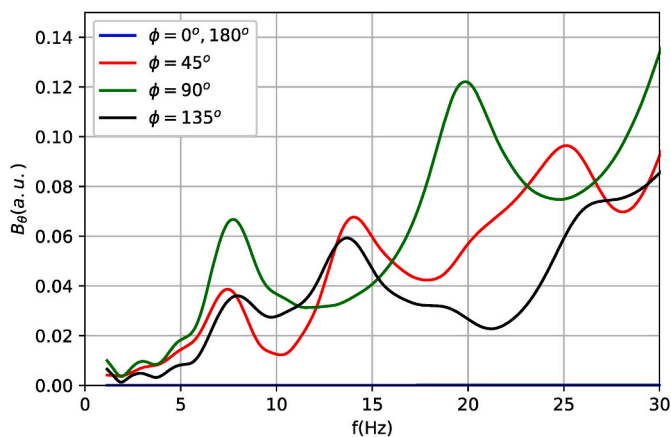


Fig. 9. NS magnetic field versus frequency for two simultaneous sources, one at ground level and the other at an altitude of 60 km with $\theta = 90^\circ$ and $\varphi = 0^\circ$. Output points are defined at ground level, $\theta = 45^\circ$ and several values of φ , from 0° to 180° .

among other applications. Besides the purely scientific knowledge, technical applications are possible. Equipment optimization, appropriate measurement campaign planning or design of assessment numerical tools to objectively calibrate the effect of environmental or sustainability engineering projects can be derived basing on the results provided with the presented code.

6. Conclusions

This work begins with a brief discussion on the interest in the study of the electromagnetic propagation in the Earth's atmosphere at the ELF band and some of its applications. The model presented considers the system as a spherical shell formed by two conducting boundaries to implement the Earth's crust and the lower ionosphere, filled with a lossy dielectric, the atmosphere. The challenging point in the numerical model relies in the fact that the radial dimension is two orders of magnitude lower than the other two dimensions. A numerical solution using the TLM method is proposed and its main aspects are presented in section 3. The algorithm is implemented through a parallelized Fortran code using OpenMP directives, with some pre-processing and post-processing parts written in Python. The code is provided and could be of interest to the scientific community working in electrodynamic aspects concerning planetary atmospheres.

The code is organized in three parts: i) input stage, ii) pre-processing stage, and iii) the TLM algorithm itself. The main aspects of each part are shortly explained to allow the use or even the modification of the provided code by other researchers. Different profiles usually considered in the specialized literature are implemented. Numerical results for Gaussian excitations and different conductivity profiles are presented in Section 5 to illustrate the code performances.

It is worth noting that the fundamental point in the presented code is the second stage. This part reindexes the original nodes in a large cubic box, converting a 3D scheme to a 1D model which only stores the interesting nodes, those between the large but close concentric shells. This procedure is key to considerably reduce the storage and CPU requirements of such a demanding numerical problem and allow spatial resolutions of around 10 km in the Earth's case, which is an appropriated size for most SR results.

Summarizing, the algorithm described here, together with the codes provided, make it possible a variety of studies. Arbitrary resolution can be achieved, limited only by computational capabilities. Any type of atmospheric conductivity profile accounting for different situations such as level of humidity, temperature, etc., can be included. In addition, local atmospheric disturbances caused, for instance, by volcano eruptions, solar activity, nuclear disasters, pollution, etc., can be modeled using the algorithm. In addition, the codes presented make it possible to study electromagnetic propagation in other planetary environments, including solar system and exoplanet atmospheres.

Code availability section

Name of the code/library: Earth TLM.

Contact: asalinas@ugr.es; +34 958242312.

Hardware requirements: Earth_TLM package has been developed on a Mac with an Apple M2 Pro processor with 16 GB RAM and 10 CPU cores. For the examples presented in this paper, the program "Earth_TLM_main.f95" uses about 8 GB and "Earth_TLM_MoiT".f95 about 5 GB. The CPU time for 100 temporal steps is 107 s when 1 core is used and 27 s when 10 cores are used.

Program language: Python and Fortran 95.

Software required: Python, Jupyter notebooks, gfortran (OpenMP)

Program size: The source codes and a Jupyter notebook with a shortened example have a size of 0.2 MB approximately. The zip file with the source codes and the Jupyter notebooks with all the cases considered in this paper has a size of 68 MB approximately. Intermediate files have a size around 2.8 GB.

The source codes and a shortened case are available for downloading at the link: https://github.com/asalinas62/Earth_TLM.git. The source codes and Jupyter notebooks with the cases studied in this paper can be downloaded, in a zip file, from the following link, located at University of Granada (Spain): <https://hdl.handle.net/10481/84341>.

Authorship contribution statement

A. Salinas: conceived and designed the analysis, developed the code, performed the analysis and wrote the original manuscript.

J. Portí: conceived and designed the analysis, developed the code and wrote the original manuscript.

E. A. Navarro: conceived, designed and performed the analysis.

S. Toledo-Redondo: conceived and designed the analysis, developed the code and provided project resources.

I. Albert: provided software supervision and participated in essential manuscript reviews and editing.

A. Castilla: provided software supervision and participated in essential manuscript reviews and editing.

V. Montagud-Camps: provided software supervision and participated in essential manuscript reviews and editing.

Declaration of competing interest

The authors declare that they have no known competing financial interests or personal relationships that could have appeared to influence the work reported in this paper.

Data availability

No data was used for the research described in the article.

Acknowledgments

We acknowledge support of MCIN/AEI 10.13039/501100011033 (grant PID 2020-112805 GA-I00)

Grant PID 2020-112805 GA-I00 funded by MCIN/AEI/10.13039/501100011033.

References

- Balsler, M., Wagner, C.A., 1962. On frequency variations of the Earth-ionosphere cavity modes. *J. Geophys. Res.* 67 (10), 4081–4083. <https://doi.org/10.1029/JZ067i010p04081>.
- Besser, B.P., 2007. Synopsis of the historical development of Schumann resonances. *Radio Sci.* 42 (2), RS2S02. <https://doi.org/10.1029/2006RS003495>.
- Blanchard, C., Portí, J., Morente, J.A., Salinas, A., Wu, B.-I., 2008. Numerical determination of frequency behavior in cloaking structures based on L-C distributed networks with TLM method. *Opt Express* 16 (13), 9344–9350. <https://doi.org/10.1364/OE.16.009344>.
- Bozóki, T., Prácer, E., Sántori, G., Dálya, G., Kapás, K., Takátsy, J., 2019. Modeling Schumann resonances with schuppy. *J. Atmos. Sol. Terr. Phys.* 196, 105144. <https://doi.org/10.1016/j.jastp.2019.105144>.
- Bozóki, T., Sántori, G., Williams, E., Mironova, I., Steinbach, P., Bland, E.C., Koloskov, A., Yampolski, Y.M., Budanov, O.V., Neska, M., Sinha, A.K., Rawat, R., Sato, M., Beggan, C.D., Toledo-Redondo, S., Liu, Y., Boldi, R., 2021. Solar cycle-modulated deformation of the earth-ionosphere cavity. *Front. Earth Sci.* 9, 735. <https://doi.org/10.3389/feart.2021.689127>.
- Christopoulos, C., 1995. In: York, N., Press, O.U. (Eds.), *The Transmission-Line Modeling Method: TLM*. The Institute of Electrical and Electronic Engineers.
- Cooray, V., 2003. *The Lightning Flash*. IET.
- Cummer, S.A., 2000. Modeling electromagnetic propagation in the Earth-ionosphere waveguide. *IEEE Trans. Antenn. Propag.* 48 (9), 1420–1429. <https://doi.org/10.1109/8.898776>.
- de Cogan, D., 1998. *Transmission Line Matrix TLM Techniques for Diffusion Applications*. Gordon and Breach.
- Fornieles-Callejón, J., Salinas, A., Toledo-Redondo, S., Portí, J., Méndez, A., Navarro, E. A., Morente-Molinera, J.A., Soto-Aranaz, C., Ortega-Cayuela, J.S., 2015. Extremely low frequency band station for natural electromagnetic noise measurement. *Radio Sci.* 50, 191–201. <https://doi.org/10.1002/2014RS005567>.
- Füllekrug, M., Fraser-Smith, A.C., 1997. Global lightning and climate variability inferred from ELF magnetic field variations. *Geophys. Res. Lett.* 24 (19), 2411–2414. <https://doi.org/10.1029/97GL02358>.
- Galuk, Y.P., Kudintseva, I.G., Nickolaenko, A.P., Hayakawa, M., 2019. Scattering of ELF radio waves by a localized non-uniformity in the lower ionosphere. *J. Atmos. Sol. Terr. Phys.* 194, 105093. <https://doi.org/10.1016/j.jastp.2019.105093>.
- Galuk, Y.P., Kudintseva, I.G., Nickolaenko, A.P., Hayakawa, M., 2020. Modifications of Schumann resonance spectra as an estimate of causative earthquake magnitude: the model treatment. *J. Atmos. Sol. Terr. Phys.* 209, 105392. <https://doi.org/10.1016/j.jastp.2020.105392>.
- Hayakawa, M., Otsuyama, T., 2002. FDTD analysis of ELF wave propagation in inhomogeneous subionospheric waveguide models. *Appl. Comput. Electromagn. Soc. J.* 239–244.
- Holland, R., 1983. THREDS: a finite-difference time-domain emp code in 3D spherical coordinates. *IEEE Trans. Nucl. Sci.* 30 (6), 4592–4595. <https://doi.org/10.1109/TNS.1983.4333177>.
- Ijeh, A.A., Cueille, M., Dubard, J.-L., Ney, M.M., 2021. Dispersion and stability analysis for TLM unstructured block meshing. *IEEE Trans. Microw. Theor. Tech.* 69 (10), 4352–4365. <https://doi.org/10.1109/TMTT.2021.3093417>.
- Johns, P.B., 1987. A symmetrical condensed node for the TLM method. *Microwave Theory Tech., IEEE Trans. On* 35 (4), 370–377.
- Kirillov, V.V., 1996. Two-dimensional theory of ELF electromagnetic wave propagation in the Earth-ionosphere waveguide channel. *Radiophys. Quantum Electron.* 39 (9), 737–743. <https://doi.org/10.1007/BF02120854>.
- Koley, S., 2023. Arsenic calamity in India's West Bengal: a critical review of mitigation scenarios. *Proc. Ins. Civil Eng. - Eng. Sustain.* 176 (4), 198–213. <https://doi.org/10.1680/jensu.21.00066>.
- Koloskov, A.V., Nickolaenko, A.P., Yampolski, Y.M., Hall, C., Budanov, O.V., 2020. Variations of global thunderstorm activity derived from the long-term Schumann resonance monitoring in the Antarctic and in the Arctic. *J. Atmos. Sol. Terr. Phys.* 201, 105231. <https://doi.org/10.1016/j.jastp.2020.105231>.
- Kulak, A., Zięba, S., Micek, S., Nieckarz, Z., 2003. Solar variations in extremely low frequency propagation parameters: 1. A two-dimensional telegraph equation (TDTE) model of ELF propagation and fundamental parameters of Schumann resonances. *J. Geophys. Res.: Space Phys.* 108 (A7). <https://doi.org/10.1029/2002JA009304>.
- Madden, T., Thompson, W., 1965. Low-frequency electromagnetic oscillations of the Earth-ionosphere cavity. *Rev. Geophys.* 3 (2), 211–254. <https://doi.org/10.1029/RG003i002p0211>.
- Marchenko, V., Kulak, A., Mlynarczyk, J., 2022. Finite-difference time-domain analysis of ELF radio wave propagation in the spherical Earth-ionosphere waveguide and its validation based on analytical solutions. *Ann. Geophys.* 40 (3), 395–406. <https://doi.org/10.5194/angeo-40-395-2022>.
- Molina-Cuberos, G.J., Morente, J.A., Besser, B.P., Portí, J., Lichtenegger, H., Schwingenschuch, K., Salinas, A., Margineda, J., 2006. Schumann resonances as a tool to study the lower ionospheric structure of Mars. *Radio Sci.* 41, RS1003.
- Morente, J.A., Giménez, G., Portí, J.A., Khalladi, M., 1995. Dispersion analysis for a TLM mesh of symmetrical condensed nodes with stubs. *IEEE Trans. Microw. Theor. Tech.* 43 (2), 452–456. <https://doi.org/10.1109/22.348108>.
- Morente, J.A., Molina-Cuberos, G.J., Portí, J.A., Besser, B.P., Salinas, A., Schwingenschuch, K., Lichtenegger, H., 2003a. A numerical simulation of Earth's electromagnetic cavity with the Transmission Line Matrix method: Schumann resonances. *J. Geophys. Res.: Space Phys.* 108 (A5). <https://doi.org/10.1029/2002JA009779>.
- Morente, J.A., Molina-Cuberos, G.J., Portí, J.A., Schwingenschuch, K., Besser, B.P., 2003b. A study of the propagation of electromagnetic waves in Titan's atmosphere with the TLM numerical method. *Icarus* 162, 374–384.
- Navarro, E.A., Soriano, A., Morente, J.A., Portí, J.A., 2007. A finite difference time domain model for the Titan ionosphere Schumann resonances. *Radio Sci.* 42 (2). <https://doi.org/10.1029/2006RS003490>.
- Navarro, E.A., Soriano, A., Morente, J.A., Portí, J.A., 2008. Numerical analysis of ionosphere disturbances and Schumann mode splitting in the Earth-ionosphere cavity. *J. Geophys. Res.: Space Phys.* 113 (A9). <https://doi.org/10.1029/2008JA013143>.
- Nickolaenko, A.P., Hayakawa, M., 2002. *Resonances in the Earth-Ionosphere Cavity*. Kluwer Acad., Dordrecht, Netherlands.
- Nickolaenko, A.P., Hayakawa, M., 2014. *Schumann Resonance for Tyros*. Springer, Japan.
- Nickolaenko, A.P., Koloskov, A.V., Hayakawa, M., Yampolski, Yu M., Budanov, O.V., Korepanov, V.E., 2015. 11-year solar cycle in Schumann resonance data as observed in Antarctica. *Sun and Geosphere* 10 (1), 39–49.
- Otsuyama, T., Sakuma, D., Hayakawa, M., 2003. FDTD analysis of ELF wave propagation and Schumann resonances for a subionospheric waveguide model. *Radio Sci.* 38 (6). <https://doi.org/10.1029/2002RS002752>.
- Paul, J., Christopoulos, C., Thomas, D.W.P., 1999a. Generalized material models in TLM - I. Materials with frequency-dependent properties. *Antennas Propagat., IEEE Trans.* 47 (10), 1528–1534.
- Paul, J., Christopoulos, C., Thomas, D.W.P., 1999b. Generalized material models in TLM - II. Materials with anisotropic properties. *Antennas Propagat., IEEE Trans.* 47 (10), 1535–1542.
- Paul, J., Christopoulos, C., Thomas, D.W.P., 2002. Generalized material models in TLM - part 3: materials with nonlinear properties. *Antennas Propagat., IEEE Trans.* 50 (7), 997–1004.
- Portí, J.A., Morente, J.A., 2001. A three-dimensional symmetrical condensed TLM node for acoustics. *J. Sound Vib.* 241 (2), 207–222. <https://doi.org/10.1006/jsvi.2000.3292>.
- Portí, J.A., Morente, J.A., Khalladi, M., Gallego, A., 1992. Comparison of thin-wire models for TLM method. *Electron. Lett.* 28 (20), 1910–1911.
- Portí, J.A., Salinas, A., Navarro, E.A., Rodríguez-Camacho, J., Fornieles, J., Toledo-Redondo, S., 2021. A new approach to the modeling of anisotropic media with the transmission line Matrix method. *Electronics* 10 (17). <https://doi.org/10.3390/electronics10172071>. Article 17.
- Prácer, E., Bozóki, T., Sántori, G., Williams, E., Guha, A., Yu, H., 2019. Reconstruction of global lightning activity based on Schumann resonance measurements: model description and synthetic tests. *Radio Sci.* 54 (3), 254–267. <https://doi.org/10.1029/2018RS006772>.
- Price, C., 2016. ELF electromagnetic waves from lightning: the Schumann resonances. *Atmosphere* 7 (9), 116. <https://doi.org/10.3390/atmos7090116>.
- Rodríguez-Camacho, J., Salinas, A., Carrión, M.C., Portí, J., Fornieles-Callejón, J., Toledo-Redondo, S., 2022. Four year study of the Schumann resonance regular variations using the sierra Nevada station ground-based magnetometers. *J. Geophys. Res. Atmos.* 127 (6), e2021JD036051. <https://doi.org/10.1029/2021JD036051>.
- Rycroft, M.J., Harrison, R.G., Nicoll, K.A., Mareev, E.A., 2008. An overview of Earth's global electric circuit and atmospheric conductivity. *Space Sci. Rev.* 137, 83–105.
- Salinas, A., Portí, J., Fornieles, J., Toledo-Redondo, S., Navarro, E.A., Morente-Molinera, J.A., 2015. TLM nodes: a new look at an old problem. *IEEE Trans. Microw. Theor. Tech.* 63 (8), 2449–2458. <https://doi.org/10.1109/TMTT.2015.2446972>.
- Salinas, A., Toledo-Redondo, S., Navarro, E.A., Fornieles-Callejón, J., Portí, J.A., 2016. Solar storm effects during Saint Patrick's Days in 2013 and 2015 on the Schumann resonances measured by the ELF station at Sierra Nevada (Spain). *J. Geophys. Res.: Space Phys.* 121 (12), 2016JA023253. <https://doi.org/10.1002/2016JA023253>.
- Sántori, G., Rycroft, M., Benzec, P., Márcz, F., Bór, J., Barta, V., Nagy, T., Kovács, K., 2013. An overview of thunderstorm-related research on the atmospheric electric field, Schumann resonances, sprites, and the ionosphere at sopron, Hungary. *Surv. Geophys.* 34 (3), 255–292. <https://doi.org/10.1007/s10712-013-9222-6>.
- Sántori, G., Williams, E., Price, C., Boldi, R., Koloskov, A., Yampolski, Y., et al., 2016. Effects of energetic solar emissions on the earth-ionosphere cavity of Schumann

- resonances. *Surv. Geophys.* 37 (4), 757–789. <https://doi.org/10.1007/s10712-016-9369-z>.
- Schumann, W.O., 1952. Über die strahlungslosen Eigenschwingungen einer leitenden Kugel die von einer Luftschicht und einer Ionosphäre umgeben ist. *Z. Naturforsch.* 7a, 149–154. <https://doi.org/10.1515/zna-1952-0202>.
- Simões, F., Pfaff, R., Berthelier, J.-J., Klenzing, J., 2012. A review of low frequency electromagnetic wave phenomena related to tropospheric-ionospheric coupling mechanisms. *Space Sci. Rev.* 168 (1–4), 551–593. <https://doi.org/10.1007/s11214-011-9854-0>.
- Simpson, J.J., Taflove, A., 2002. Two-dimensional FDTD model of antipodal ELF propagation and Schumann resonance of the Earth. *IEEE Antenn. Wireless Propag. Lett.* 1, 53–56. <https://doi.org/10.1109/LAWP.2002.805123>.
- Simpson, J.J., Taflove, A., 2004. Three-dimensional FDTD modeling of impulsive ELF propagation about the Earth-sphere. *IEEE Trans. Antenn. Propag.* 52 (2), 443–451. <https://doi.org/10.1109/TAP.2004.823953>.
- Simpson, J.J., Taflove, A., 2007. A review of progress in FDTD Maxwell's equations modeling of impulsive subionospheric propagation below 300 kHz. *IEEE Trans. Antenn. Propag.* 55 (6), 1582–1590. <https://doi.org/10.1109/TAP.2007.897138>.
- Smith, D.R., Padilla, W.J., Vier, D.C., Nemat-Nasser, S.C., Schultz, S., 2000. Composite medium with simultaneously negative permeability and permittivity. *Phys. Rev. Lett.* 84 (18), 4184–4187. <https://doi.org/10.1103/PhysRevLett.84.4184>.
- Soriano, A., Navarro, E.A., Morente, J.A., Portí, J.A., 2007. A numerical study of the Schumann resonances in Mars with the FDTD method. *J. Geophys. Res.: Space Phys.* 112 (A6) <https://doi.org/10.1029/2007JA012281>.
- Soriano, A., Navarro, E.A., Paul, D.L., Portí, J.A., Morente, J.A., Craddock, I.J., 2005. Finite difference time domain Simulation of the Earth-ionosphere resonant cavity: Schumann resonances. *IEEE Trans. Antenn. Propag.* 53 (4), 1535–1541. <https://doi.org/10.1109/TAP.2005.844415>.
- Toledo-Redondo, S., Salinas, A., Fornieles, J., Portí, J., Lichtenegger, H.I.M., 2016. Full 3-D TLM simulations of the Earth-ionosphere cavity: effect of conductivity on the Schumann resonances. *J. Geophys. Res.: Space Phys.* 121 (6), 2015JA022083 <https://doi.org/10.1002/2015JA022083>.
- Toledo-Redondo, S., Salinas, A., Morente-Molinera, J.A., Méndez, A., Fornieles, J., Portí, J., Morente, J.A., 2013. Parallel 3D-TLM algorithm for simulation of the Earth-ionosphere cavity. *J. Comput. Phys.* 236, 367–379. <https://doi.org/10.1016/j.jcp.2012.10.047>.
- Toledo-Redondo, S., Salinas, A., Portí, J., Witasse, O., Cardnell, S., Fornieles, J., Molina-Cuberos, G.J., Déprez, G., Montmessin, F., 2017. Schumann resonances at Mars: effects of the day-night asymmetry and the dust-loaded ionosphere. *Geophys. Res. Lett.* 44 (2), 2016GL071635 <https://doi.org/10.1002/2016GL071635>.
- Tronchoni, A.B., Bretas, A.S., Gazzana, D.S., 2019. Two-dimensional Transmission Line Modeling method: an algorithm considering non-homogeneous media and ionization. *Elec. Power Syst. Res.* 173, 220–229. <https://doi.org/10.1016/j.epr.2019.04.035>.
- Williams, E.R., 1992. The Schumann Resonance: a global tropical thermometer. *Science* 256 (5060), 1184–1187. <https://doi.org/10.1126/science.256.5060.1184>.
- Williams, E., Bozóki, T., Sántori, G., Price, C., Steinbach, P., Guha, A., Liu, Y., Beggan, C. D., Neska, M., Boldi, R., Atkinson, M., 2021. Evolution of global lightning in the transition from cold to warm phase preceding two super El niño events. *J. Geophys. Res. Atmos.* 126 (3), e2020JD033526 <https://doi.org/10.1029/2020JD033526>.
- Williams, E.R., Mushtak, V., Guha, A., Boldi, R., Bór, J., Nagy, T.G., Sántori, G., 2014. Inversion of multi-station Schumann resonance background records for global lightning activity in absolute units. *AGU Fall Meeting Abstracts 1*, AE24A-08.
- Yang, H., Pasko, V.P., 2005. Three-dimensional finite difference time domain modeling of the Earth-ionosphere cavity resonances. *Geophys. Res. Lett.* 32 (3), L03114 <https://doi.org/10.1029/2004GL021343>.
- Yang, H., Pasko, V.P., Yair, Y., 2006. Three-dimensional finite difference time domain modeling of the Schumann resonance parameters on Titan, Venus, and Mars. *Radio Sci.* 41 (2), RS2S03. <https://doi.org/10.1029/2005RS003431>.
- Yu, Y., Niu, J., Simpson, J.J., 2012. A 3-D global earth-ionosphere FDTD model including an anisotropic magnetized plasma ionosphere. *IEEE Trans. Antenn. Propag.* 60 (7), 3246–3256. <https://doi.org/10.1109/TAP.2012.2196937>.
- Ziolkowski, R.W., Kipple, A.D., 2003. Causality and double-negative metamaterials. *Phys. Rev.* 68 (2), 026615 <https://doi.org/10.1103/PhysRevE.68.026615>.